

## High-mobility bottom-contact *n*-channel organic transistors and their use in complementary ring oscillators

Byungwook Yoo, Taeho Jung, Debarshi Basu, and Ananth Dodabalapur<sup>a)</sup>

*Microelectronics Research Center, The University of Texas at Austin, 10100 Burnet Road, Building 160, Austin, Texas 78758*

Brooks A. Jones, Antonio Facchetti, Michael R. Wasielewski, and Tobin J. Marks

*Department of Chemistry, the Materials Research Center, and the Center for Nanofabrication & Molecular Self-Assembly, Northwestern University, 2145 Sheridan Road, Evanston, Illinois 60208-3113*

(Received 26 September 2005; accepted 18 January 2006; published online 22 February 2006)

The electrical characteristics of bottom-contact organic field-effect transistors fabricated with the air-stable *n*-type semiconductor *N,N'*-bis(*n*-octyl)-dicyanoperylene-3,4:9,10-bis(dicarboximide) (PDI-8CN<sub>2</sub>) are described. The mobility, threshold voltage, subthreshold swing, and  $I_{\text{on}}/I_{\text{off}}$  ratio ( $V_{\text{DS}}=40$  V,  $V_{\text{G}}=0\sim 40$  V) are 0.14 cm<sup>2</sup>/V s, 1.6 V, 2.0 V/decade, and  $1.2\times 10^3$ , respectively. The effect of electrode/dielectric surface treatment on these devices is also examined, with a combination of 1-octadecanethiol and hexamethyldisilazane. Organic complementary five-stage ring oscillators were fabricated using pentacene and PDI-8CN<sub>2</sub>, and operated at an oscillation frequency of 34 kHz and a propagation delay per stage of 3 μs. © 2006 American Institute of Physics. [DOI: 10.1063/1.2177627]

Organic field effect transistors (OFETs) have attracted considerable attention for use in applications such as radio-frequency identification tags, display drivers, smart cards, and sensor arrays.<sup>1-3</sup> The investigation and development of materials that can be used in *n*-channel organic transistors is crucial for the development of practical organic electronics. Some of the earliest reports of *n*-channel organic transistors used electron-deficient perylene and naphthalene-based semiconductors with good electrical properties and even ambient device stability with *N*-fluoroalkyl functionalization.<sup>4,5</sup> As the understanding of charge transport in organic materials advances, materials from the oligothiophene, fullerene, and rylene imide families having top-contact mobilities consistently in excess of 0.1 cm<sup>2</sup> V<sup>-1</sup> s<sup>-1</sup> have been reported.<sup>6-12</sup> Notable among high performance *n*-type materials, the perylene diimide (PDI) family holds the distinction of having one of the highest *n*-type mobilities known of 0.6 cm<sup>2</sup> V<sup>-1</sup> s<sup>-1</sup> uncorrected for contact resistance and 1.7 cm<sup>2</sup> V<sup>-1</sup> s<sup>-1</sup> when corrected.<sup>9</sup> In addition to the outstanding electrical properties, PDI-based materials have demonstrated great promise due to their ability to yield semiconducting films from solution and air-stable device operation.<sup>10</sup> The latter characteristics arise from cyano group addition to the perylene core (*N,N'*-bis(*n*-octyl)-dicyanoperylene-3,4:9,10-bis(dicarb-oximide), PDI-8CN<sub>2</sub>), which increases solubility by decreasing molecular planarity and stabilizes charge carriers by lowering the energies of the lowest unoccupied molecular orbitals associated with electron transport.

Most reports on *n*-channel organic transistors use the top-contact geometry, in which the source and drain contacts are defined on top of the semiconductor by shadow masking.<sup>6,7,9,10</sup> The channel lengths created using shadow masking are typically large (>25 μm) and unsuitable for fabricating fast circuits. In order to achieve the performance required for practical electronics, shorter channel lengths (<10 μm) are required. The fabrication of such structures is

best accomplished in the bottom-contact configuration, in which the source and drain electrodes are first defined and the semiconductor is deposited on top of the electrodes. Most studies of bottom-contact *n*-channel OFETs employ large channel length devices ( $\geq 50$  μm) in which the contact injection requirements are reduced.<sup>12,13</sup> The use of self-assembled monolayers (SAM) at the interface between the metal/insulator and the semiconductor results in improved properties by lowering surface energy differences. The most common agent for passivating the hydrophilic inorganic substrates is hexamethyldisilazane (HMDS), which coats the SiO<sub>2</sub> surface with a lower surface energy trimethylsilyl monolayer. Thiol-based SAMs have also been employed for passivation of gold source and drain electrodes.<sup>14-17</sup> In particular, 1-octadecanethiol (ODT) has proven useful for modifying the surface energy of gold electrodes to facilitate charge carrier injection.

In this letter we report on the results of surface treatments on the electrical characteristics of bottom-contact transistors fabricated with the air-stable *n*-type semiconductor PDI-8CN<sub>2</sub>. With careful surface passivation, the bottom-contact mobility of PDI-8CN<sub>2</sub> (0.14 cm<sup>2</sup> V<sup>-1</sup> s<sup>-1</sup>) is nearly equal to the top-contact mobility (0.16 cm<sup>2</sup> V<sup>-1</sup> s<sup>-1</sup>). The mobility we obtain—0.14 cm<sup>2</sup> V<sup>-1</sup> s<sup>-1</sup>—is the highest reported for bottom-contact *n*-channel organic transistors with channel lengths <5 μm. Utilizing the unique electrical properties of PDI-8CN<sub>2</sub>, five-stage complementary ring oscillators with PDI-8CN<sub>2</sub> *n*-channel FETs and pentacene *p*-channel FETs have been fabricated.

The bottom-contact structure of the *n*-channel PDI-8CN<sub>2</sub> OFETs is shown in Fig. 1(a). The substrate is a heavily doped *p*-type silicon substrate serving as the gate electrode, with 100 nm of thermally grown SiO<sub>2</sub> as the dielectric layer (34.5 nF/cm<sup>2</sup>). The e-beam evaporated electrodes comprised of a 2.5 nm Ti adhesion layer and a 35 nm Au layer were photolithographically patterned with channel widths (*W*) and lengths (*L*) of 200 and 4 μm, respectively. Prior to the PDI-8CN<sub>2</sub> deposition, three kinds of surface treatments were

<sup>a)</sup>Electronic mail: ananth@mail.utexas.edu

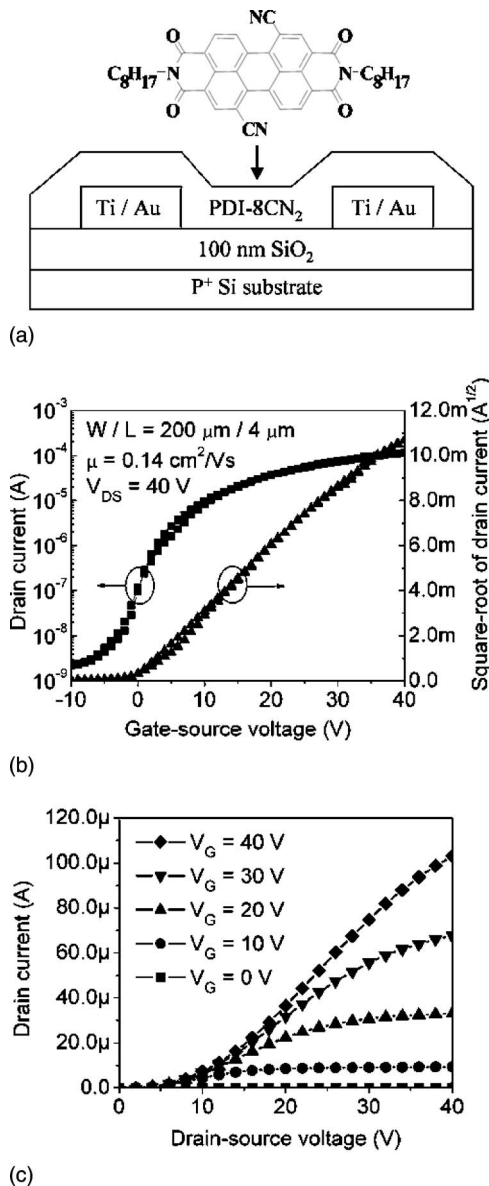


FIG. 1. (a) The structure of a bottom-contact OFET device. The chemical structure of PDI-8CN<sub>2</sub> is also shown. (b) Transfer characteristics of 4 μm channel length ( $W/L=50$ ) OFETs. The gate bias was swept from negative to positive voltage. (c) Output characteristics of 4 μm channel length ( $W/L=50$ ) OFETs.

performed; HMDS only, ODT only, and HMDS followed by ODT. The final fabrication step was thermal deposition of a 45 nm PDI-8CN<sub>2</sub> film. The PDI-8CN<sub>2</sub> had previously been purified by chromatography on silica and multiple recrystallizations. During the deposition at a base vacuum of  $4.5 \times 10^{-7}$  Torr, the substrates were maintained at 100 °C to enhance the PDI-8CN<sub>2</sub> grain growth, and the deposition rate was 0.2–0.7 Å/s. In the case of the complementary ring oscillator, PDI-8CN<sub>2</sub> and pentacene were used as *n*-channel and *p*-channel materials, respectively, due to their high mobility and ease of use. Both HMDS and 1-hexadecanethiol (HDT) treatments were also performed. The deposition conditions for PDI-8CN<sub>2</sub> films were the same as the transistor fabrication above. Pentacene films were thermally deposited onto a 60 °C substrate to a thickness of 42 nm. The base pressure was  $4 \times 10^{-7}$  Torr and the deposition rate was 0.2–0.8 Å/s. All electrical characterizations were carried out under vacuum ( $\sim 1$  mTorr) at 300 K.

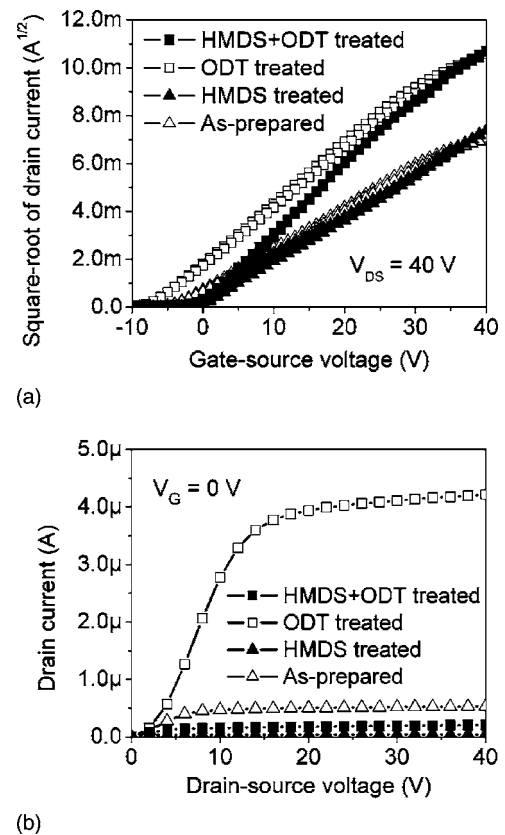


FIG. 2. (a) Square root of drain current vs gate voltage characteristics at a source/drain voltage equal to 40 V for as-prepared (open triangle), HMDS-treated (filled triangle), ODT-treated (open square), and HMDS+ODT treated (filled square) FETs with channel length  $L=4 \mu\text{m}$  and width  $W=200 \mu\text{m}$ . (b) Output characteristics of OFETs at zero gate bias for as-prepared (open triangle), HMDS-treated (filled triangle), ODT-treated (open square), and HMDS+ODT treated (filled square) FETs.

The transfer and output characteristics of representative PDI-8CN<sub>2</sub> transistors treated with both HMDS and ODT are shown in Figs. 1(b) and 1(c), respectively. Noticeable hysteresis is not found in the transfer characteristics; however, the current is still injection limited in the low drain voltage region despite ODT treatment. The saturation mobility, the threshold voltage, and subthreshold swing are  $0.14 \text{ cm}^2 \text{ V}^{-1} \text{ s}^{-1}$ , 1.6 V, and 2.0 V/decade, respectively.  $I_{\text{on}}/I_{\text{off}}$  ratio ( $V_{\text{DS}}=40 \text{ V}$ ,  $V_{\text{G}}=0 \sim 40 \text{ V}$ ) is  $1.2 \times 10^3$  and  $I_{\text{on}}/I_{\text{off}}$  ratio ( $V_{\text{DS}}=40 \text{ V}$ ,  $V_{\text{G}}=-10 \sim 40 \text{ V}$ ) is  $5.7 \times 10^4$ . Such  $I_{\text{on}}/I_{\text{off}}$  ratios are typical of cyanated PDI semiconductors.<sup>10</sup>

Figure 2(a) shows  $\sqrt{I_{\text{D}}}$  versus  $V_{\text{G}}$  plots at the source-drain voltage of 40 V for devices fabricated with four different surface treatments. No noticeable improvement of mobility is observed on HMDS-treated SiO<sub>2</sub> surface functionalized samples; however, mobility is enhanced by about one order of magnitude for ODT-treated (Au surface functionalized) samples. The output characteristics of the samples at zero gate bias, shown in Fig. 2(b), reveal that the off current of the ODT-treated samples is greater than that of the HMDS-treated samples by approximately two orders of magnitude, which results in a low  $I_{\text{on}}/I_{\text{off}}$  ratio for the ODT-treated samples. The mobility, threshold voltage, and current on/off ratio for variously treated OTFTs are summarized in Table I. The threshold voltage is slightly positive for HMDS-treated and HMDS+ODT treated devices. If additional charge is created on the SiO<sub>2</sub> surface by HMDS treatment, the charge

TABLE I. Comparison of mobility, threshold voltage, and current on/off ratio for OFETs having various treatments

Condition	Mobility ( $\text{cm}^2 \text{V}^{-1} \text{s}^{-1}$ )	$V_{TH}$ (V)	$I_{on}/I_{off}$ ratio ( $V_{DS}=40 \text{ V}$ , $V_G=0-40 \text{ V}$ )
As-prepared	$3.9 \times 10^{-2}$	-1.9	$1.1 \times 10^2$
HMDS treatment	$4.4 \times 10^{-2}$	2.0	$2.8 \times 10^3$
Octadecanethiol treatment	$7.5 \times 10^{-2}$	-6.4	$3.7 \times 10^1$
HMDS+octadecanethiol	0.14	1.6	$1.2 \times 10^3$

carrier concentration can be influenced, thus affecting the threshold voltage.<sup>18</sup>

The complementary metal-oxide-semiconductor (CMOS) circuit, which consists of both *p*-channel and *n*-channel transistors, is an ideal circuit configuration for organic semiconductors because it has low static power dissipation. The maximum switching frequency of a single transistor is a function of the mobility, terminal voltages, and channel length. The schematic of a five-stage ring oscillator is shown in Fig. 3(a). The operating frequency of the ring oscillator is an indicator of the maximum speed at which the digital circuits can be used. Figure 3(b) shows the oscillation frequency characteristics with a supplying voltage of 100 V and a channel length of 7.5  $\mu\text{m}$ . An oscillation frequency of 34 kHz was achieved with a propagation delay per stage of  $\sim 3 \mu\text{s}$ . Although a higher oscillation frequency was recently reported for the *p*-channel MOS configuration,<sup>19</sup> the present result is the highest oscillation frequency reported for an organic CMOS configuration.<sup>3,20</sup> The improved performance of this device is due to the significant improvement of the *n*-channel mobility; however, the mobility of the *n*-channel is still somewhat lower than that of the *p*-channel. The ring oscillator frequency will be improved by increasing the mo-

bility of the *n*-channel further as well as reducing channel lengths and overlap capacitances between the source/drain electrodes and the gate.

In summary, we demonstrated that PDI-8CN<sub>2</sub> is a suitable *n*-channel material for bottom-contact OFET devices. From the *I*-*V* characteristics, the mobility, the threshold voltage, subthreshold swing,  $I_{on}/I_{off}$  ratio ( $V_{DS}=40 \text{ V}$ ,  $V_G=0 \sim 40 \text{ V}$ ), and  $I_{on}/I_{off}$  ratio ( $V_{DS}=40 \text{ V}$ ,  $V_G=-10 \sim 40 \text{ V}$ ) were determined to be  $0.14 \text{ cm}^2 \text{V}^{-1} \text{s}^{-1}$ , 1.6 V, 2.0 V/decade,  $1.2 \times 10^3$ , and  $5.7 \times 10^4$ , respectively. The highest mobility result was obtained with HMDS-treated SiO<sub>2</sub> gate dielectric and ODT-treated Au electrodes. Based on these results, a substantial improvement in organic CMOS ring oscillators has been demonstrated. Using pentacene and PDI-8CN<sub>2</sub>, an oscillation frequency of 34 kHz was obtained in a five-stage ring oscillator. With additional material/device optimization, the speeds of this type of ring oscillator should be enhanced even further.

The authors gratefully acknowledge support from the AFOSR (STTR FA 9550-04-0080), the NSF through an NIRT (ECS-021698), the NASA Institute for Nanoelectronics and Computing (NCC2-3163), ONR (N00014-05-1-0021), and NSF through the Northwestern MRSEC (DMR-0076097). The authors also acknowledge helpful support from OrganicID, Inc.

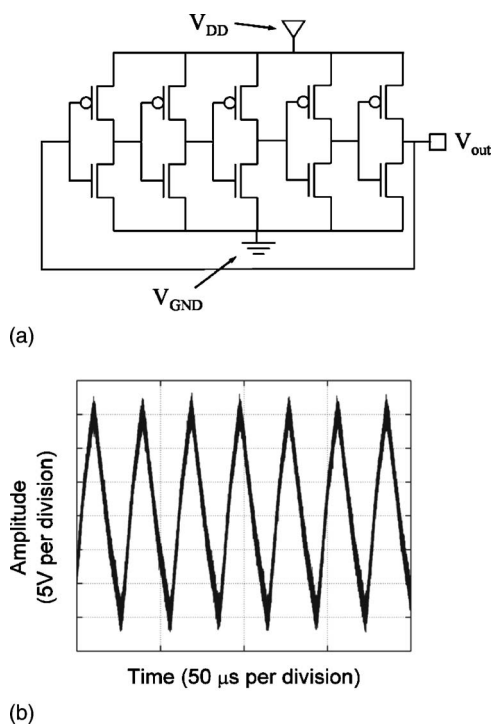


FIG. 3. (a) Schematic of a five complementary ring oscillator without buffer stage. (b) Oscillation of 34 kHz in a ring oscillator with  $V_{supply}=100 \text{ V}$ .

<sup>1</sup>Z. N. Bao, Adv. Mater. (Weinheim, Ger.) **12**, 227 (2000).

<sup>2</sup>C. D. Dimitrakopoulos and D. J. Mascaró, IBM J. Res. Dev. **45**, 11 (2001).

<sup>3</sup>B. K. Crone, A. Dodabalapur, R. Sarpeshkar, R. W. Filas, Y. Y. Lin, Z. Bao, J. H. O'Neill, W. Li, and H. E. Katz, J. Appl. Phys. **89**, 5125 (2001).

<sup>4</sup>J. R. Osctrick, A. Dodabalapur, L. Torsi, A. J. Lovinger, E. W. Kwock, T. M. Miller, M. Galvin, M. Berggren, and H. E. Katz, J. Appl. Phys. **81**, 6804 (1997).

<sup>5</sup>J. G. Laquindanum, H. E. Katz, A. Dodabalapur, and A. J. Lovinger, J. Am. Chem. Soc. **118**, 11331 (1996).

<sup>6</sup>H. E. Katz, A. J. Lovinger, J. Johnson, C. Kloc, T. Siegrist, W. Li, Y.-Y. Lin, and A. Dodabalapur, Nature (London) **404**, 478 (2000).

<sup>7</sup>M.-H. Yoon, S. A. DiBenedetto, A. Facchetti, and T. J. Marks, J. Am. Chem. Soc. **127**, 1348 (2005).

<sup>8</sup>J. A. Letizia, A. Facchetti, C. L. Stern, M. A. Ratner, and T. J. Marks, J. Am. Chem. Soc. **127**, 13476 (2005).

<sup>9</sup>R. J. Chesterfield, J. C. Mckeen, C. R. Newman, P. C. Ewbank, D. A. da Silva Filho, J.-L. Bredas, L. L. Miller, K. R. Mann, and C. D. Frisbie, J. Phys. Chem. B **108**, 19281 (2004).

<sup>10</sup>B. A. Jones, M. J. Ahrens, M.-H. Yoon, A. Facchetti, T. J. Marks, and M. R. Wasielewski, Angew. Chem., Int. Ed. **43**, 6363 (2004).

<sup>11</sup>A. Babel and S. A. Jenekhe, J. Am. Chem. Soc. **125**, 13656 (2003).

<sup>12</sup>P. R. L. Malenfant, C. D. Dimitrakopoulos, J. D. Gelorme, L. L. Kosbar, T. O. Graham, A. Curioni, and W. Andreoni, Appl. Phys. Lett. **80**, 2517 (2002).

<sup>13</sup>S. Kobayashi, T. Takenobu, S. Mori, A. Fujiwara, and Y. Iwasa, Appl. Phys. Lett. **82**, 4581 (2003).

<sup>14</sup>F. F. Fan, J. Yang, L. Cai, D. W. Price, Jr., S. M. Dirk, D. V. Kosynkin, Y. Yao, A. M. Rawlett, J. M. Tour, and A. J. Bard, J. Am. Chem. Soc. **124**, 5550 (2002).

<sup>15</sup>I. Kymissis, C. D. Dimitrakopoulos, and S. Purushothaman, IEEE Trans. Electron Devices **48**, 1060 (2001).

<sup>16</sup>A. Salleo, M. L. Chabinyc, M. S. Yang, and R. A. Street, Appl. Phys. Lett. **81**, 4383 (2002).

<sup>17</sup>D. J. Gundlach, L. L. Jia, and T. N. Jackson, IEEE Electron Device Lett. **22**, 571 (2001).

<sup>18</sup>K. P. Pernstich, C. Goldmann, C. Krellner, D. Oberhoff, D. J. Gundlach, and B. Batlogg, Synth. Met. **146**, 325 (2004).

<sup>19</sup>W. Clemens, W. Fix, J. Ficker, A. Knobloch, and A. Ullmann, J. Mater. Res. **19**, 1963 (2004).

<sup>20</sup>H. Klauk, M. Halik, U. Zschieschang, F. Eder, D. Rohde, G. Schmid, and C. Dehm, IEEE Trans. Electron Devices **52**, 618 (2005).